

## The Challenge of Wide-Field Transit Surveys: The Case of GSC 01944-02289

Georgi Mandushev<sup>1</sup>, Guillermo Torres<sup>2</sup>, David W. Latham<sup>2</sup>, David Charbonneau<sup>2,3</sup>, Roi Alonso<sup>4</sup>, Russel J. White<sup>3</sup>, Robert P. Stefanik<sup>2</sup>, Edward W. Dunham<sup>1</sup>, Timothy M. Brown<sup>5</sup>, and Francis T. O'Donovan<sup>3</sup>

### ABSTRACT

Wide-field searches for transiting extra-solar giant planets face the difficult challenge of separating true transit events from the numerous false positives caused by isolated or blended eclipsing binary systems. We describe here the investigation of GSC 01944-02289, a very promising candidate for a transiting brown dwarf detected by the Transatlantic Exoplanet Survey (TrES) network. The photometry and radial velocity observations suggested that the candidate was an object of substellar mass in orbit around an F star. However, careful analysis of the spectral line shapes revealed a pattern of variations consistent with the presence of another star whose motion produced the asymmetries observed in the spectral lines of the brightest star. Detailed simulations of blend models composed of an eclipsing binary plus a third star diluting the eclipses were compared with the observed light curve and used to derive the properties of the three components. Using the predicted stellar parameters we were able to identify a second set of spectral lines corresponding to the primary of the eclipsing binary and derive its spectroscopic orbit. Our photometric and spectroscopic observations are fully consistent with a blend model of a hierarchical triple system composed of an eclipsing binary with G0V and M3V components in orbit around a slightly evolved F5 dwarf. The rotational broadening of the spectral lines of the F5 primary ( $v \sin i \approx 34 \text{ km s}^{-1}$ ) and its brightness relative to the eclipsing binary ( $\sim 89\%$  of the total light) made the discovery of the true nature of the system particularly difficult. We believe that this investigation will be helpful to other groups pursuing wide-field transit searches as this type of false detection could be more common than true transiting planets, and difficult to identify.

---

<sup>1</sup>Lowell Observatory, 1400 W. Mars Hill Rd., Flagstaff, AZ 86001, USA; gmand@lowell.edu; Ted.Dunham@lowell.edu

<sup>2</sup>Harvard-Smithsonian Center for Astrophysics, 60 Garden St., Cambridge, MA 02138, USA; gtorres@cfa.harvard.edu; dlatham@cfa.harvard.edu; dcharbonneau@cfa.harvard.edu; rstefanik@cfa.harvard.edu

<sup>3</sup>California Institute of Technology, MC 105-24, 1200 E. California Blvd., Pasadena, CA 91125, USA; rjw@astro.caltech.edu; ftod@astro.caltech.edu

<sup>4</sup>Instituto de Astrofísica de Canarias, C/ vía Láctea s/n, 38200 La Laguna, Tenerife, Spain; ras@iac.es

<sup>5</sup>High Altitude Observatory, National Center for Atmospheric Research, P.O. Box 3000, Boulder, CO 80307, USA; timbrown@hao.ucar.edu

*Subject headings:* binaries: eclipsing — line: profiles — planetary systems — techniques: photometric — techniques: radial velocities

## 1. Introduction

Nearly all of the more than 130 known extrasolar planets<sup>1</sup> have been discovered by means of radial velocity observations. Such observations provide no information on the planet’s size, and, because of the unknown orbital inclination, only a lower limit on the mass of the planet can be established. One of the most important results from the radial velocity planet detections was that the extrasolar planetary systems discovered so far are very different from the solar system, with massive (and presumably large) Jupiter-like planets orbiting very close (less than 0.1 AU) to their central stars.

Long before the initial discoveries of extrasolar planets around Sun-like stars by the Doppler technique (Latham et al. 1989; Mayor & Queloz 1995), it was recognized that planets around other stars could also be detected photometrically if they cross in front of their parent stars producing transits (Struve 1952). Transit observations can provide the missing planet size information and in combination with radial velocity data they can be used to derive the planet’s density and infer its composition. The realization that there could be many extrasolar Jupiter-like planets in short-period orbits led to the development of a number of ground-based, wide-field photometric searches for transiting planets<sup>2</sup>. In those surveys many thousands of relatively bright stars ( $9 \lesssim R \lesssim 13$ ) are monitored for periodic shallow drops in the star brightness caused by a transiting planet. The expected amplitude of the drop and duration of the transit are 1%–2% and 2–4 hr, respectively, for a Jupiter-sized planet in a 2–7 day orbit around a Sun-like star. Recent advances in instrumentation and data analysis allow measurements of the stellar brightness with milli-magnitude precision over a period of several weeks or months with small, relatively inexpensive and automated telescopes. Indeed, the Transatlantic Exoplanet Survey (TrES) network recently announced the first successful detection of a transiting planet using a wide-field, small-aperture transit survey (Alonso et al. 2004).

Confirmation of the planetary nature of the transit candidates still requires follow-up radial velocity observations with larger telescopes since photometry alone cannot distinguish true planetary transits from transit-like events produced by other astronomical phenomena (Brown 2003; Latham 2003; Charbonneau et al. 2004). Common impostors are eclipsing binaries in which the secondary is much smaller than the primary, or systems with components undergoing grazing eclipses. In both cases the radial velocity amplitudes are tens of kilometers per second, and usually only a few low-precision ( $\sim 1 \text{ km s}^{-1}$ ) radial-velocity measurements are enough to reveal the stellar nature of

---

<sup>1</sup>Extrasolar Planets Catalog (<http://cfa-www.harvard.edu/planets/catalog.html>), maintained by Jean Schneider.

<sup>2</sup>Transit Search Programmes (<http://star-www.st-and.ac.uk/~kdh1/transits/table.html>), maintained by Keith Horne.

the companions. In other cases more subtle analyses of the photometric and spectroscopic data are needed to ascertain that the transit candidate is in fact a planet (see, e.g., Konacki et al. 2003; Torres et al. 2004a,b).

While there is very little published observational data on the rate of false alarms in wide-field transit surveys, the statistics in Dunham et al. (2004) and the preliminary results from the Vulcan survey (Latham 2003) indicate that the frequency of false positives is very high, probably 20 or more times the number of true planetary transits. In the case of TrES-1, the only transiting planet discovered in such a survey (Alonso et al. 2004), the ratio of transit candidates to true planets was 25:1. Therefore, it is to be expected that most of the transit candidates in any photometric survey will be false positives and careful follow-up work is crucial in establishing their true nature.

In this paper we describe the case of GSC 01944-02289, a relatively bright ( $V \simeq 10.4$ ) star in Cancer that initially appeared to be a very good candidate for a transiting brown dwarf. The transit light curves and the radial velocity observations were consistent with a  $0.03M_{\odot}$  brown dwarf in a 3.35 day orbit around an F5 star. However, further analysis shows that this is not a transiting brown dwarf, but instead a blend of an eclipsing binary and a slightly evolved F5 star in a hierarchical triple system.

## 2. Wide-Field Photometry

A  $6^{\circ} \times 6^{\circ}$  field centered on  $\chi$  Cancri was observed with the Lowell Observatory automated Planet Search Survey Telescope (PSST) between 2003 February 3 and April 26. This telescope is part of TrES, with telescopes at Palomar Observatory (USA), Lowell Observatory (USA), and Instituto de Astrofísica de Canarias (Spain). The PSST is a 105 mm f/2.8 refractor equipped with a  $2K \times 2K$  CCD and is described fully in Dunham et al. (2004). Nearly all exposures were taken through a Kron-Cousins  $R$  filter with the exception of several hundred  $B$  and  $V$  images on 2003 March 7 and 8 that were used to estimate stellar colors. A total of 4894  $R_C$  exposures were used in the photometric analysis after the rejection of images of questionable quality. All  $R_C$  images have an exposure time of 90 s.

Our photometric reduction pipeline is built around the difference image analysis (DIA) approach described in Alard (2000). The complete pipeline is explained in detail in Dunham et al. (2004); here we outline only the principal steps.

All images were flat-fielded and overscan- and bias-subtracted using the appropriate tasks in the IRAF<sup>3</sup> package (Tody 1993). One of the images taken at low airmass on a moonless photometric night was chosen as the reference image for the field, and profile-fitting photometry was carried out for that image using Peter Stetson’s DAOPHOT II/ALLSTAR suite (Stetson 1987, 1992). After

---

<sup>3</sup>IRAF is distributed by the National Optical Astronomy Observatory, which is operated by the Association of Universities for Research in Astronomy, Inc., under cooperative agreement with the National Science Foundation.

deriving the geometric transformations between the reference image and all other images, all images were resampled to the pixel grid of the reference image. A master frame for the field was constructed by co-adding 19 good-quality images and all other images were subtracted from this master frame to produce the difference images. The next step was to carry out aperture photometry on the difference images using the centroids from the profile-fitting photometry of the reference image. The result was a time series of 4894 magnitude differences  $\Delta m_i = -2.5 \log[(F_0 - \Delta F_i)/F_0]$  for each star in the master list for the field, where  $F_0$  and  $\Delta F_i$  are the aperture fluxes of the star in the master and the  $i$ th difference image, respectively. The last step was to decorrelate the light curves by regressing each light curve against the light curves of  $\sim 250$  other stars, a technique very similar to that described in Jenkins et al. (2000). Average light curves were constructed by binning the decorrelated data in 0.0062 day ( $\sim 9$  minute)-wide bins. The typical scatter in the photometry of the brightest stars, as measured by the rms, is  $\sim 0.005$  mag before and  $\sim 0.002$  mag after the binning.

About 8000 stars with low enough scatter ( $\text{RMS} \leq 0.02$  mag after the binning) were searched for transit events using the box least squares (BLS) algorithm (Kovács et al. 2002). The algorithm assumes only two levels in the periodic light curve, and thus is more efficient than generic methods that search for any periodic variation. It performs very well in low signal-to-noise ratio (S/N) situations and is generally capable of detecting transit signals with amplitude of about 6 times the rms or better. The light curves of the eight transit candidates identified by the BLS search were examined visually to eliminate possible false detections such as stars with signs of a secondary eclipse or continuously varying light curve. We estimate that the visual inspection can detect secondary eclipses or modulated light curves with amplitudes as low as 0.006–0.01 mag.

One of the best transit candidates was GSC 01944-02289 (J2000 coordinates:  $\alpha = 08^{\text{h}}26^{\text{m}}22^{\text{s}}.56$ ,  $\delta = +26^{\circ}59'45''.5$ ). Its binned light curve, folded with the photometric period of 3.35 days, is shown in Figure 1. Each filled circle in the plot is the weighted average of up to five individual measurements. Two complete and two partial transit-like events with a depth of 1.4% and duration of 2.7 hours were observed. The Two Micron All Sky Survey (2MASS) colors of the object were typical for an F dwarf and examination of the Digitized Sky Survey<sup>4</sup> images did not show any bright companions inside the  $\sim 20''$  PSST stellar profile. Based on the shape and duration of the transit, and the preliminary spectral type from the 2MASS catalog, GSC 01944-02289 was classified as a probable transit candidate and was included in the radial-velocity monitoring program with the Harvard-Smithsonian Center for Astrophysics (CfA) Digital Speedometers (Latham 1985, 1992). We also initiated a program of photometric and spectroscopic observations with larger telescopes, both to try to improve the photometric precision and to determine whether the transit-like events were truly caused by a dark substellar object.

---

<sup>4</sup>The Digitized Sky Survey was produced at the Space Telescope Science Institute under U.S. Government grant NAG W-2166. The images of these surveys are based on photographic data obtained using the Oschin Schmidt Telescope on Palomar Mountain and the UK Schmidt Telescope. The plates were processed into the present compressed digital form with the permission of these institutions.

### 3. Multicolor Photometry

The principal motivation for obtaining multicolor photometry was two-fold: to check for color-dependent depth of the transit (which in some cases would indicate a stellar and not a substellar companion) and to obtain standard magnitudes and colors for the primary star. In addition we wanted to confirm the stellar parameters derived from the low-resolution CfA spectra that were already available at that time.

We obtained off-transit  $BV(RI)_C$  exposures on 2004 March 26 and in-transit  $BVI_C$  exposures on 2004 March 27 (UT dates) with the Lowell Observatory 42'' (105-cm) Hall reflector in combination with a  $2K \times 2K$  SITe CCD. Aperture photometry was carried out on all images to derive the instrumental magnitudes. We used the mean magnitude of several comparison stars in each exposure to correct for the effects of atmospheric extinction, varying seeing, etc., and to produce the differential  $BVI_C$  light curves for GSC 01944-02289. During the off-transit observations on 2004 March 26, we also observed four photometric standards in the SA101 and G163 fields (Landolt 1992) in order to calibrate the photometry.

We also obtained in-transit  $VI_J$  photometry on 2004 April 2 with the Instituto de Astrofísica de Canarias (IAC) 82-cm telescope equipped with a  $1K \times 1K$  CCD. Because of the smaller field of view ( $7' \times 7'$ ), only one comparison star was used to obtain the final differential photometry. The mean error of a single observation was  $\sim 0.007$  mag in  $V$  and  $\sim 0.006$  mag in  $I$ .

The transit light curves from 2004 March 27 (Lowell) and 2004 April 2 (IAC) are shown in Figure 2. Each plot is labeled with the filter and date of observation. The data were binned in the same way as the wide-field photometry, i.e., using bin widths of 0.0062 days; therefore each point in the plot is the weighted average of up to three individual measurements. On both nights the observations were affected by cirrus and the moon. Nevertheless, the photometry is good enough to ascertain that the depth of the transit-like events is equal within the observational errors in all three filters. A statistically significant difference in the transit depths (after accounting for limb darkening) would have rejected this object as a transit candidate. Equal depths, however, do not preclude the possibility of stellar companions of similar colors and low luminosity. The precision of our multicolor photometry is not enough to detect the effect of limb darkening with certainty: the expected transit depth difference for a solar-type star is  $\sim 0.003$  mag between the  $B$  and  $I$  light curves (Seager & Mallén-Ornelas 2003) and could be even less for a hotter F star.

The observations of two full transits roughly a year after the PSST photometry from 2003 also allowed us to refine the system's photometric period and derive an improved transit ephemeris:

$$\text{Min I (HJD)} = (2452676.3021 \pm 0.0005) + (3.35002 \pm 0.00002)E \quad (1)$$

where  $E$  is the number of whole periods elapsed since the reference transit epoch.

In Table 1 we have summarized the principal properties of the transit candidate as derived from our wide-field and multi-color photometry, as well as the  $JHK$  photometry from the 2MASS catalog.

## 4. Spectroscopic Observations

The transit candidate was observed spectroscopically at high resolution and high S/N at the Keck Observatory, and also with similar resolution but lower S/N at the CfA for the purpose of monitoring the radial velocity of the star. We describe these observations below.

### 4.1. Keck Observations and Results

Observations of GSC 01944-02289 with the Keck I telescope were obtained on 2004 April 3 during the course of another program using the HIRES instrument (Vogt et al. 1994). Two exposures of 10 and 20 minutes were obtained, together with exposures of a telluric standard and three spectral standards with accurately known radial velocities (see Table 2). The instrument was used with the red collimator and an RG-610 filter at cross-disperser angle of  $1^{\circ}40'05''$  and echelle angle of  $-0^{\circ}28'60''$ . The D1 decker ( $1''.15 \times 14''.0$ ) has a projected width of 4 pixels and produced spectra at  $\lambda/\Delta\lambda = 34,000$ . Sixteen echelle orders, each with a length of  $\sim 100 \text{ \AA}$ , were recorded in the wavelength interval 6330–8750  $\text{\AA}$ , with gaps between orders. Exposures of an internal quartz lamp for flat-fielding and a ThAr lamp for wavelength calibration were also made with the same setup. The spectra were extracted using the MAKEE package written by Tom Barlow, and then resampled onto a uniform logarithmic wavelength scale. The radial and projected rotational velocities of GSC 01944-02289 were determined via a cross-correlation analysis with the three spectral standards listed in Table 2, resulting in values of  $RV = +31.4 \pm 0.4 \text{ km s}^{-1}$  and  $v \sin i = 33.8 \pm 0.6 \text{ km s}^{-1}$ . For the cross correlations, we used 10 spectral regions of length 20–30  $\text{\AA}$  that contained no prominent telluric absorption features or strong gravity sensitive features like K I at 7665 and 7699  $\text{\AA}$ , Na I at 8183 and 8195  $\text{\AA}$ , or Ca II at 8498  $\text{\AA}$ .

To estimate stellar parameters from the HIRES spectra, we obtained the atlas of synthetic spectra (based on the Kurucz ATLAS9 models) presented recently by Zwitter et al. (2004). We used a restricted grid of parameters, spanning  $5000 < T_{\text{eff}} < 7500$ ,  $2.5 < \log g < 5.0$ , and  $-0.5 < [\text{M}/\text{H}] < 0.5$ , where  $T_{\text{eff}}$  is in K and the surface gravity  $\log g$  is in  $\text{cm s}^{-2}$ . Microturbulent velocity was fixed at  $2 \text{ km s}^{-1}$  and the rotational velocity  $v \sin i$  at  $30 \text{ km s}^{-1}$ , the model grid-point closest to the estimated value of  $34 \text{ km s}^{-1}$ . We repeated the analysis described below with models at  $40 \text{ km s}^{-1}$  and did not derive significantly different results. We interpolated the model spectra onto the wavelength solution for the HIRES data corrected for the system velocity. Telluric absorption features were identified in the observed spectrum of a rapidly-rotating A-star calibrator, and data at these wavelengths were given zero statistical weight in the subsequent analysis.

Five HIRES echelle orders overlapped with the spectral range of the models and were relatively free of telluric absorption: 7679–7791  $\text{\AA}$ , 7850–7964  $\text{\AA}$ , 8028–8145  $\text{\AA}$ , 8410–8533  $\text{\AA}$ , and 8615–8741  $\text{\AA}$ . For each of these echelle orders  $n$ , we calculated the  $\chi^2$  difference  $\chi_n^2(T_{\text{eff}}, \log g)$  between each model spectrum (multiplied by a low-order polynomial to correct for the residuals in flattening the blaze function of the spectrograph) and the observed data. We then summed the  $\chi_n^2$  values at each  $T_{\text{eff}}$

and  $\log g$  over the five spectral orders  $n$ . We also considered models at  $[M/H] = \pm 0.5$ , both of which yielded significantly poorer fits to the data. The majority of the spectral features constrain primarily the temperature. However, our spectral range also encompasses two lines (at 8498 and 8662 Å) from the Ca II triplet that yield good constraints on the surface gravity. Two portions of the spectrum in the vicinity of the Ca triplet features are shown in Figure 3 and overplotted with model spectra.

The formal  $\chi^2$  errors are not representative of the true uncertainties, since the theoretical spectra reveal systematic differences from the observed data (due to missing features or uncertainties in the line parameters). To evaluate the uncertainties in the stellar parameters, we repeated the above analysis for two of the spectral standard stars in Table 2, HD 78154A and HD 84737. We first rotationally broadened the observed spectra to  $30 \text{ km s}^{-1}$  to simulate any degradation in the parameter estimation for GSC 01944-02289 due to its rapid rotation. Based on the accuracy of the model fits to these spectral standards, and a visual inspection of the model fits (see Figure 3), we estimate  $T_{\text{eff}} = 6600 \pm 150 \text{ K}$  and  $\log g = 4.3 \pm 0.5$  for GSC 01944-02289, consistent with an F5V star ( $M \simeq 1.3M_{\odot}$ ,  $R \simeq 1.3R_{\odot}$ ).

## 4.2. CfA Observations and Results

Spectroscopic monitoring of GSC 01944-02289 was conducted at the CfA with the 1.5-m Tillinghast reflector at the F. L. Whipple Observatory (Mount Hopkins, Arizona), and the 1.5-m Wyeth reflector at the Oak Ridge Observatory (Harvard, Massachusetts), over a period of 3 months between 2004 February and May. Identical echelle spectrographs with photon-counting Reticon detectors were used on both telescopes, giving a resolving power of  $\lambda/\Delta\lambda = 35,000$ . A single echelle order spanning  $45 \text{ Å}$  was recorded at a central wavelength of  $5187 \text{ Å}$ , which includes the Mg b triplet. A total of 33 spectra were obtained, with S/Ns ranging from about 14 to 35 per resolution element of  $8.5 \text{ km s}^{-1}$ .

Radial velocities were measured by cross-correlation using the IRAF task XCSAO (Kurtz & Mink 1998). The template was selected from a large library of synthetic spectra based on model atmospheres by R. L. Kurucz,<sup>5</sup> computed for us by J. Morse. The parameters of the template are the effective temperature, rotational velocity, and surface gravity, with the first two affecting the velocities the most. Solar metallicity was assumed throughout. The values best matching the star were determined from grids of cross-correlations, seeking the highest correlation averaged over all exposures. The formal values are  $T_{\text{eff}} = 6200 \pm 200 \text{ K}$ ,  $\log g = 3.5 \pm 0.5$ , and  $v \sin i = 34 \pm 2 \text{ km s}^{-1}$ , although temperature and gravity are strongly correlated owing to the narrow spectral window. The rotational velocity agrees well with the estimate from the Keck spectra, while the temperature is somewhat lower. In view of the correlation mentioned above we adopted a compromise value

---

<sup>5</sup>Available at <http://cfaku5.cfa.harvard.edu>.

of  $T_{\text{eff}} = 6500$  K, corresponding roughly to an F5 star. For the gravity we adopted  $\log g = 4.0$ . The radial velocities we obtained, using the synthetic template from our library closest to these parameters, have internal errors around  $1 \text{ km s}^{-1}$ , which in our experience is quite typical for stars with this rotational broadening. Instrumental shifts affecting the velocities were monitored and corrected for by obtaining frequent exposures of the twilight sky, as described by Latham (1992).

The radial velocities show a clear pattern of variation with the same period as the photometry (Eq.[1]), and a phasing that is consistent with what is expected for transits (negative slope at phase 0.0, which corresponds to the epoch of the transit). This suggests orbital motion. A Keplerian orbit (assumed to be circular owing to the short period) adjusted to these data is shown in Figure 4, where the ephemeris has been adopted from photometry and held fixed. The velocity semi-amplitude of  $K = 3.55 \pm 0.21 \text{ km s}^{-1}$  is highly significant. If due to orbital motion, the minimum mass of the companion is determined to be  $M_2 \sin i = (0.0250 \pm 0.0030)(M_1 + M_2)^{2/3} M_{\odot}$ , where  $M_1$  is the mass of the star and  $i$  is the inclination angle of the orbit. With a typical mass for an F5 main sequence star of  $M_1 \approx 1.3M_{\odot}$  and an orbit that is essentially edge-on as implied by the transits, this corresponds to a companion mass of  $\sim 32 M_{\text{Jup}}$ , which is clearly in the brown dwarf regime. The center-of-mass velocity of the system is  $+35.30 \pm 0.15 \text{ km s}^{-1}$ , and the rms residual from the fit is  $0.88 \text{ km s}^{-1}$ .

While the discovery of a bona-fide brown dwarf companion to a solar-type star in such a tight orbit would certainly be of great interest, finding one that also transits across the disk of its parent star would be unprecedented and would allow for the first time the measurement of the size and mean density of such an object directly. The observational evidence presented above for GSC 01944-02289 is fairly typical of what other transit surveys and subsequent follow-up work might produce, and no obvious signs are seen that would indicate a false positive detection (see also Section 5.3). For example, visual examination of the spectra and of the corresponding cross-correlation functions revealed no sign of lines from another star that might be causing spurious velocity variations. Furthermore, there is no significant wavelength dependence to the depth of the transits (see Section 3), which would be expected in general if more than one star is involved. In view of the importance of this case, however, we undertook a series of other tests described below. These ultimately proved that the star is, in fact, *not* orbited by a brown dwarf companion, but instead that both the photometric and the spectroscopic signatures are the result of blending with an eclipsing binary. We present these tests in some detail as an example of the care required to validate transit candidates that are being generated by these kinds of searches.

## 5. Identifying A False Positive

One of the potentially observable manifestations of a blend scenario is periodic changes in the shapes of the spectral lines due to contamination from the eclipsing binary, which may give the impression of radial velocity variations in the brighter star. Although different in nature, this is qualitatively similar to the effect produced by chromospheric activity in more active stars, which

can also produce spurious velocity variations (see, e.g., Queloz et al. 2001).

Direct spectroscopic detection of the eclipsing binary in GSC 01944-02289 may be more difficult, particularly if it is faint. However, additional information on the properties of the configuration can be obtained from detailed modeling of the light curve, and this can significantly constrain the problem and aid in the disentangling of the spectral features of the binary, even allowing the measurement of its radial velocity. We focus below on the CfA spectroscopy that provides the better time coverage, and we explore these issues in turn.

### 5.1. Line Shapes

Beyond the visual inspection of the spectra and cross-correlation functions for GSC 01944-02289 described in the previous section, a much more sensitive measure of the presence of contaminating lines from another star can be obtained by examining the profiles of the spectral lines for asymmetries. These asymmetries can be quantified by measuring the “bisector spans,” usually defined as the velocity difference between the top and bottom of the line bisectors (see, e.g., Queloz et al. 2001; Torres et al. 2004a) or between any other two reference levels. We have computed these here for our CfA spectra directly from the cross-correlation functions, which can be taken to represent the profile of the average spectral line in the star. Figure 5 shows the individual line bisectors from our spectra, along with the bisector spans plotted as a function of the photometric phase, based on the ephemeris from Eq.[1]. We note that the magnitude of the asymmetries in GSC 01944-02289 is substantially larger than in the Sun, where lines typically show spans of only a few hundred meters per second. The rather obvious trend with phase is a strong indication of contamination by the lines of another star, moving back and forth with respect to the (presumably) fixed lines of the F star with a period of 3.35 days. Thus, changes in the line asymmetry appear to have resulted in spurious velocity variations due to the measuring technique, which uses a significant portion of the line profile.<sup>6</sup> The pattern of the variations (first negative, then positive) is the same as that of the velocities in Figure 4. The implication is that the line-profile changes are due to the primary of an eclipsing binary along the same line of sight. Blending with the brighter star dilutes the normal eclipses and reduces their depth to the level that we see, only 1.4%.

### 5.2. Modeling The Light Curve As A Triple Star System

To constrain further the properties of the blend and derive properties for the eclipsing binary that will help in the direct detection of its lines in the spectra of GSC 01944-02289, we turn next to the photometry. We model the *R*-band light curve as a combination of the light from

---

<sup>6</sup>The radial velocity is determined in XCSAO as the centroid of the peak of the cross-correlation function, from a quadratic fit to the top 50% of the peak. Thus, asymmetries in the profile will affect the centroid directly.

an eclipsing binary plus a brighter third star, following Torres et al. (2004b). Briefly, the light variations (not only the depth and duration of the transit, but also the detailed shape) are modeled with a combination of three stars whose properties are parameterized in terms of their mass. All other stellar properties are derived from model isochrones, which can be the same for the eclipsing binary and the third star if they form a physical triple system, or different otherwise. The mass of the brightest star in the system is constrained by the spectroscopic and photometric information available (see Section 4), mainly the effective temperature of 6500 K. These light-curve fits are usually not unique. However, once the masses for the stars composing the eclipsing binary are determined from the fit, other properties of the blend can be predicted that can potentially be tested against the observations, such as the brightness of the eclipsing binary relative to the brightest star (amount of dilution), the orbital velocity amplitudes of the eclipsing binary, and the projected rotational velocities of its components (for details see Torres et al. 2004b). As we show below the powerful combination of the photometric and spectroscopic constraints typically resolves the ambiguities, and allows one to arrive at a single configuration that agrees with all the observations.

Light-curve modeling of a physical triple system (all stars at the same distance) assuming that the brightest star is an F5 main-sequence object resulted in a good fit to the observations but implied an eclipsing binary that is far too bright to be missed in our spectra. Placing the binary in the background to make it fainter (thus removing the condition of physical association with the F star) resulted in fits that were also acceptable. However, the near-sinusoidal pattern of line asymmetries in Figure 5 suggests that if there is another star in the spectrum, its center-of-mass velocity must be fairly close to the mean velocity of GSC 01944-02289. Although not impossible, this would be rather unlikely for a line-of-sight alignment of unrelated stars. We, therefore, explored other possibilities in which the F star is intrinsically brighter.

The spectroscopic constraint we have on the surface gravity of GSC 01944-02289 is such that a modest degree of evolution cannot be ruled out by the observations (see Section 4). Because of the morphology of the isochrones in the vicinity of the turnoff, it is possible within certain ranges of age and temperature for an evolved F star to be significantly brighter at any given temperature (by up to 2 mag in some cases) if it is near the end of its main-sequence life, beyond the turnoff point. The mass will obviously be considerably larger than a star located before the turnoff at the same  $T_{\text{eff}}$  (see Figure 7 below). Our estimate of the effective temperature for GSC 01944-02289 happens to be in the range that allows this ambiguity.

Extensive light-curve modeling under this scenario resulted in a solution for a triple system providing an excellent fit to the photometry, with an eclipsing binary (composed of a G0 star orbited by an M3 star) roughly an order of magnitude fainter than the slightly evolved F5 star, consistent with the detection limits from our visual inspection of the spectra. This fit is shown in Figure 6. The secondary eclipse seen in the plot has a predicted depth of only 0.002 mag, which is undetectable in our present data. The inclination angle that provides the best solution is  $87^\circ$ , and the F star contributes 89% of the total light in the  $R$  band. The properties of the three

stars composing the blend are listed in Table 3, where the mass of the F star was fixed to give a temperature in close agreement with our spectroscopic estimate of 6500 K. The age determined for the system is  $\sim 1.6$  Gyr, and the distance (ignoring extinction and forcing agreement with the total apparent magnitude in the  $R$  band) is approximately 500 pc. The location of the three stars in the H-R diagram is illustrated in Figure 7, along with model isochrones from the series by Girardi et al. (2000).

### 5.3. Spectroscopically Recovering The Eclipsing System

Given the short orbital period, the stars in the eclipsing binary are likely to have their rotation synchronized with the orbital motion due to tidal forces. For solar-type stars this would result in a line broadening of some  $15 \text{ km s}^{-1}$ . In view of the rapid rotation of the F star itself ( $v \sin i = 34 \text{ km s}^{-1}$ ), we anticipate that the lines of the G star in the eclipsing binary will essentially be always blended with those of the F star. This will make their direct detection challenging (particularly if they are faint), even knowing where to look. As an illustration we show in Figure 8 the cross-correlation functions for two of our observations of GSC 01944-02289 near the quadratures, where the velocity separation between the G star and the F star should be the largest if the modeling in the preceding section is correct. We indicate with arrows the expected location of the G star (see below), but no obvious signs of it are seen.

Modern techniques for analyzing composite spectra such as the two-dimensional cross-correlation algorithm TODCOR (Zucker & Mazeh 1994) have the potential to enable this detection, even under severe line blending, thereby providing definitive proof of a blend. In TODCOR the observed spectra are cross-correlated against a composite template made by adding together two separate templates chosen to match each star. A two-dimensional correlation function is produced by exploring all possible combinations of Doppler shifts of the two stars. The maximum of this function should occur when the Doppler shifts of the two templates match the observation. This technique effectively decouples the velocities of the two stars, overcoming the blending problems of standard one-dimensional correlation techniques. Additionally, the light ratio can be left as an additional free parameter to be determined from the same observations (see Zucker & Mazeh 1994).

The modeling in Section 5.2 predicts that the brightness of the G star (the primary star in the eclipsing binary) relative to the F star in GSC 01944-02289 is 0.12 in the  $V$  band, which is close to the central wavelength of the CfA spectra. This corresponds to  $\Delta V = 2.3$  mag. Additionally, its velocity semi-amplitude and rotational velocity are predicted to be  $39.4$  and  $16.8 \text{ km s}^{-1}$ , respectively. These values, along with the temperature and surface gravity from Table 3, provide the information needed to look for direct signs of the G star in the spectra. Using a synthetic template closely matching these parameters, along with the same template adopted earlier for the F star, we re-analyzed the CfA spectra using TODCOR. We were indeed able to detect the G star, and measure its radial velocity (as well as that of the F star) in each of our spectra. These radial velocities are listed in Table 4. An illustration of this detection is given in Figure 9, in which the

top panel shows a contour plot of the two-dimensional correlation function for one of our spectra at the second quadrature (same spectrum as in the bottom panel of Figure 8). Cross sections through the maximum of the correlation function are indicated by dotted lines, and are displayed in the lower two panels. The peak at the expected location for the G star in the bottom panel shows that the lines of that star are present in the spectrum, and allow the Doppler shift to be measured.

A Keplerian orbit adjusted to the velocities of the G star, with the ephemeris from Eq.[1] held fixed and assuming a circular orbit, gives a semi-amplitude of  $38.24 \pm 0.80 \text{ km s}^{-1}$ . This is very close to the predicted value. The center-of-mass velocity of this orbit is  $+35.71 \pm 0.59 \text{ km s}^{-1}$ , and the rms residual of the fit is  $3.36 \text{ km s}^{-1}$ . The residuals of the individual velocity measurements are listed in Table 4, along with the orbital phase. The observations and fitted orbit are shown graphically in Figure 10. Following Zucker & Mazeh (1994), we also determined the light ratio directly from our spectra. The result,  $0.12 \pm 0.02$ , is virtually identical to the predicted value.

The velocities of the F star measured with TODCOR, which previously displayed a clear variation with a semi-amplitude of  $3.5 \text{ km s}^{-1}$  (Section 4.2), are now essentially constant: the rms residual around the mean is  $0.76 \text{ km s}^{-1}$  (see Figure 10). This indicates that TODCOR has effectively removed the contamination from the primary of the eclipsing binary, which was biasing our original measurements. For reference, we include in Figure 10 the spurious orbit from Figure 4 (*dashed line*), which is seen not to fit the new measurements. We note also that the mean velocity of the F star as determined from its new velocities,  $\langle \text{RV}_F \rangle = +35.40 \pm 0.13 \text{ km s}^{-1}$ , is the same as the center-of-mass velocity of the eclipsing binary, within the errors. For a hierarchical system this similarity may be indicative of a wide orbit for the eclipsing pair around the F star, unless that orbit has a low inclination angle or we happened to measure the system at a special phase. The lack of any significant variation in the velocities of the F star over the three-month interval of our observations implies an outer period that is probably significantly longer than this.

With the eclipsing binary now confidently identified in our spectra, as a check we repeated the determination of the template parameters in the same way as done originally, but extending the technique to the case of composite spectra (see, e.g., Torres et al. 2002). Although the results are more uncertain because twice as much information is being extracted from the same spectra (the effective S/N of each star is lower), the parameters we obtained for the F star ( $T_{\text{eff}} = 6400 \text{ K}$ ,  $v \sin i = 33 \text{ km s}^{-1}$ ) are very close to what we had been using, and those for the primary of the eclipsing binary ( $T_{\text{eff}} = 5900 \text{ K}$ ,  $v \sin i = 18 \text{ km s}^{-1}$ ) are also in excellent agreement with the blend model. We point out that the latter values (which are purely spectroscopic) are essentially independent of the light-curve modeling and thus provide gratifying confirmation of the blend results.

### 5.4. System Colors

Our modeling of the  $R$ -band photometry allows us to predict the depth that the eclipses would have in other passbands, in particular in  $B$ ,  $V$ , and  $I_C$ , which we observed (see Section 3). With the blend parameters described above, all three of these filters show the same expected transit depth as in the  $R$  band to within about a milli-magnitude, a difference that is well below our detection threshold. The reason for the similarity is the small difference in color (or effective temperature) between the F star and the G star. Thus, GSC 01944-02289 represents a type of blend that is virtually impossible to expose from the wavelength dependence of the transit depth.

Finally, an additional check for self-consistency in our model is given by the comparison between the predicted total apparent magnitudes for the blend (sum of three stars) and the measured brightness of GSC 01944-02289 in a variety of passbands spanning the optical and near-infrared. This comparison is shown in Table 5. The differences between the observed and predicted magnitudes are no larger than 0.02 mag, which is quite a remarkable agreement considering all the uncertainties involved, including systematic errors in the fluxes from the evolutionary models and other errors of an observational nature.

## 6. Discussion

Current wide-field transit surveys easily achieve the required photometric precision and time coverage necessary to detect short-period transiting giant planets (see, e.g., Bakos et al. 2004; Dunham et al. 2004). Our experience is that a single  $6^\circ \times 6^\circ$  field yields anywhere from five to 20 or more transit candidates depending on the number of stars with sufficient photometric precision (from  $\sim 3000$  in fields at high Galactic latitude to more than 20000 in fields near the Galactic plane). The principal difficulty facing such surveys is the effective rejection of false alarms, such as the just described case of GSC 01944-02289 and others (e.g., Charbonneau et al. 2004). Some false positives are relatively easy to uncover using high-cadence photometry or low-precision radial velocity measurements (Latham 2003; Charbonneau et al. 2004). However, the case of GSC 01944-02289 shows that a blend of an eclipsing binary with a third star can mimic a transiting planet almost perfectly.

It has often been argued that blend configurations — perhaps the most insidious of the false positive scenarios affecting transit candidates — can usually be detected from the wavelength dependence of the transit depth. The case of GSC 01944-02289 is a poignant counterexample. As described above, the close similarity in color (temperature) between the two brightest components leads to little or no wavelength dependence. This underlines the importance of careful spectroscopic follow-up, not only to measure radial velocities but also to examine the spectral line profiles. Furthermore, it would appear that such cases may not be as rare as previously thought among certain kinds of stars. The transit candidate OGLE-TR-33, found in the course of the OGLE survey (Udalski et al. 2002a), was also shown by Torres et al. (2004b) to be a blend resulting from

a hierarchical triple system involving an eclipsing binary. In both GSC 01944-02289 and OGLE-TR-33, the brightest star is of spectral type F. This is significant, since Torres et al. (2004b) showed (see their Fig. 10) that precisely in the F stars the main sequence widens enough that it allows an evolved star to be intrinsically brighter by up to 2 mag at a given temperature, leaving ample room to hide a fainter star (the eclipsing binary) in its glare. Additionally, F stars are typically rotating quite rapidly ( $v \sin i \simeq 30\text{--}40 \text{ km s}^{-1}$  or more) and their line broadening is often similar to the orbital velocity amplitude expected for the eclipsing binary in a blend (for short periods typical of transit candidates). Under these conditions the spectral lines of the bright star and the eclipsing binary will be severely blended over much of the orbit, making it difficult to detect the latter. As a result the line asymmetries caused by contamination from the eclipsing binary will lead to spurious velocity variations measured for the bright star that are nearly sinusoidal, and therefore more easily confused with real variations. Thus, transit candidates that are F stars require extra care. Such candidates could be quite common, given that at the typical Galactic latitude ( $|b| \simeq 15^\circ$ ) of our magnitude-limited surveys the maximum of the star counts of main-sequence stars is around spectral type F5.

To date, five transiting extrasolar planets have been discovered from their photometric signatures and confirmed spectroscopically: one in a wide-field survey (TrES-1, Alonso et al. 2004), and four around stars in the OGLE-III survey (Udalski et al. 2002b,c, 2003): OGLE-TR-56 (Konacki et al. 2003), OGLE-TR-111 (Pont et al. 2004), OGLE-TR-113 (Bouchy et al. 2004; Konacki et al. 2004), and OGLE-TR-132 (Bouchy et al. 2004). They have all undergone an analysis of the bisector variations and possible blend scenarios, and so the detection of planetary companions around those stars can be considered secure. Recent spectroscopic follow-up of several OGLE transit candidates (Konacki et al. 2003; Torres et al. 2004b) demonstrates that even with stars as faint as those ( $V \sim 16$ ) the analysis technique applied here is able to distinguish between blends and true transiting planets.

We thank Mike Calkins, Perry Berlind, and Joe Zajac for obtaining many of the CfA spectra. We also thank Tomaz Zwitter for allowing us access to his unpublished atlas of Kurucz stellar atmosphere models, Peter Stetson for providing us with the DAOPHOT II package, and Phil Massey for the assistance with obtaining observing time on the 42" Hall telescope.

Some of the observations presented here were obtained at the W. M. Keck Observatory, which is operated as a scientific partnership of the California Institute of Technology, the University of California, and the National Aeronautics and Space Administration (NASA). The observatory was made possible by the generous financial support of the W. M. Keck foundation. This work was carried out in part with support from grants NAG5-8271, NAG5-12088, and NNG04LG89G under the auspices of the NASA Origins of Solar Systems Program, and the Keck PI Data Analysis Fund (JPL 1260769).

This publication makes use of data products from the Two Micron All Sky Survey, which is a joint project of the University of Massachusetts and the Infrared Processing and Analysis

Center/California Institute of Technology, funded by the National Aeronautics and Space Administration and the National Science Foundation. This research has also made use of the Simbad database operated at Centre de données astronomiques de Strasbourg, in Strasbourg, France.

## REFERENCES

- Alard, C. 2000, *A&AS*, 144, 363
- Alonso, R., Brown, T. M., Torres, G., Latham, D. W., Sozzetti, A., Mandushev, G., Belmonte, J. A., Charbonneau, D., Deeg, H. J., Dunham, E. W., O'Donovan, F. T., Stefanik, R. P. 2004, *ApJ*, 613, L153
- Bakos, G., Noyes, R. W., Kovács, G., Stanek, K. Z., Sasselov, D. D., & Domsa, I. 2004, *PASP*, 116, 266
- Brown, T. M. 2003, *ApJ*, 593, L125
- Bouchy, F., Pont, F., Santos, N. C., Melo, C., Mayor, M., Queloz, D., & Udry, S. 2004, *A&A*, 421, L13
- Carpenter, J. M. 2001, *AJ*, 121, 2851
- Charbonneau, D., Brown, T. M., Dunham, E. W., Latham, D. W., Looper, D. L., & Mandushev, G. I. 2004, in *The Search for Other Worlds*, AIP Conf. Proc. 713, eds. S. S. Holt & D. Deming, (New York: Springer-Verlag), 151
- de Medeiros, J. R., & Mayor, M. 1999, *A&AS*, 139, 433
- Dunham, E. W., Mandushev, G., Taylor, B., & Oetiker, B. 2004, *PASP*, 116, 1072
- Girardi, L., Bressan, A., Bertelli, G., & Chiosi, C. 2000, *A&AS*, 141, 371
- Jenkins, J. M., Witteborn, F., Koch, D. G., Dunham, E. W., Borucki, W. J., Updike, T. F., Skinner, M. A., & Jordan, S. P. 2000, *Proc. SPIE*, 4013, 520
- Keenan, P. C., & McNeil, R. C. 1989, *ApJS*, 71, 245
- Konacki, M., Torres, G., Sasselov, D. D., & Jha, S. 2003, *ApJ*, 597, 1076
- Konacki, M., Torres, G., Sasselov, D. D., Pietrzyński, G., Udalski, A., Jha, S., Ruiz, M. T., Gieren, W., & Minniti, D. 2004, *ApJ*, 609, L37
- Kovács, G., Zucker, C., & Mazeh, T. 2002, *A&A*, 391, 369
- Kurtz, M. J., & Mink, D. J. 1998, *PASP*, 110, 934
- Landolt, A. U. 1992, *AJ*, 104, 340
- Latham, D. W. 1985, in *Stellar Radial Velocities*, Proc. IAU Coll. 88, eds. A. G. D. Philip & David W. Latham (Schenectady: L. Davis Press), 5

- Latham, D. W. 1992, in IAU Coll. 135, Complementary Approaches to Double and Multiple Star Research, ASP Conf. Ser. 32, eds. H. A. McAlister & W. I. Hartkopfeds (San Francisco: ASP), 110
- Latham, D. W. 2003, in Scientific Frontiers in Research on Extrasolar Planets, ASP Conf. Ser. 294, eds. D. Deming & S. Seager, (San Francisco: ASP), 409
- Latham, D. W., Stefanik, R. P., Mazeh, T., Mayor, M., & Burki, G. 1989, *Nature*, 339, 38
- Mayor, M. & Queloz, D. 1995, *Nature*, 378, 355
- Nidever, D. L., Marcy, G. W., Butler, R. P., Fischer, D. A., & Vogt, S. S. 2002, *ApJS*, 141, 503
- Pont, F., Bouchy, F., Queloz, D., Santos, N. C., Melo, C., Mayor, M., & Udry, S. 2004, *A&A*, 426, L15
- Queloz, D., Henry, G. W., Sivan, J. P., Baliunas, S. L., Beuzit, J. L., Donahue, R. A., Mayor, M., Naef, D., Perrier, C., & Udry, S. 2001, *A&A*, 379, 279
- Seager, S., & Mallén-Ornelas, G. 2003, *ApJ*, 585, 1038
- Stetson, P. B. 1987, *PASP*, 99, 191
- Stetson, P. B. 1992, in *Astronomical Data Analysis Software and Systems I*, ASP Conf. Ser. 25, eds. D. M. Worrall, C. Biemesderfer, & J. Barnes (San Francisco: ASP), 297
- Struve, O. 1952, *The Observatory*, 72, 199
- Torres, G., Konacki, M., Sasselov, D. D., & Jha, S. 2004a, *ApJ*, 609, 1071
- Torres, G., Konacki, M., Sasselov, D. D., & Jha, S. 2004b, *ApJ*, 614, 979
- Torres, G., Neuhäuser, R., & Guenther, E. W. 2002, *AJ*, 123, 1701
- Tody, D. 1993, in *Astronomical Data Analysis Software and Systems II*, ASP Conf. Ser. 52, eds. R.J. Hanisch, R.J.V. Brissenden, & J. Barnes (San Francisco: ASP), 172
- Udalski, A., Paczyński, B., Żebruń, K., Szymański, M., Kubiak, M., Soszyński, I., Szewczyk, O., Wyrzykowski, L., & Pietrzyński, G. 2002a, *Acta Astron.*, 52, 1
- Udalski, A., Żebruń, K., Szymański, M., Kubiak, M., Soszyński, I., Szewczyk, O., Wyrzykowski, L., & Pietrzyński, G. 2002b, *Acta Astronomica*, 52, 115
- Udalski, A., Szewczyk, O., Żebruń, K., Pietrzyński, G., Szymański, M., Kubiak, M., Soszyński, I., & Wyrzykowski, L. 2002c, *Acta Astronomica*, 52, 317
- Udalski, A., Pietrzyński, G., Szymański, M., Kubiak, M., Żebruń, K., Soszyński, I., Szewczyk, O., & Wyrzykowski, L. 2003, *Acta Astronomica*, 53, 133

Vogt, S. S. et al. 1994, Proc. SPIE, 2198, 362

Zucker, S., & Mazeh, T. 1994, ApJ, 420, 806

Zwitter, T., Castelli, F., & Munari, U. 2004, A&A, 417, 1055

Fig. 1.— Binned  $R$  light curve of GSC 01944-02289 obtained from the wide-field photometry. The data are folded with the photometric period of 3.35 days. Only the portion near the transit times is shown. The rms over the whole observing season is  $\sim 0.0028$  mag (see Section 2).

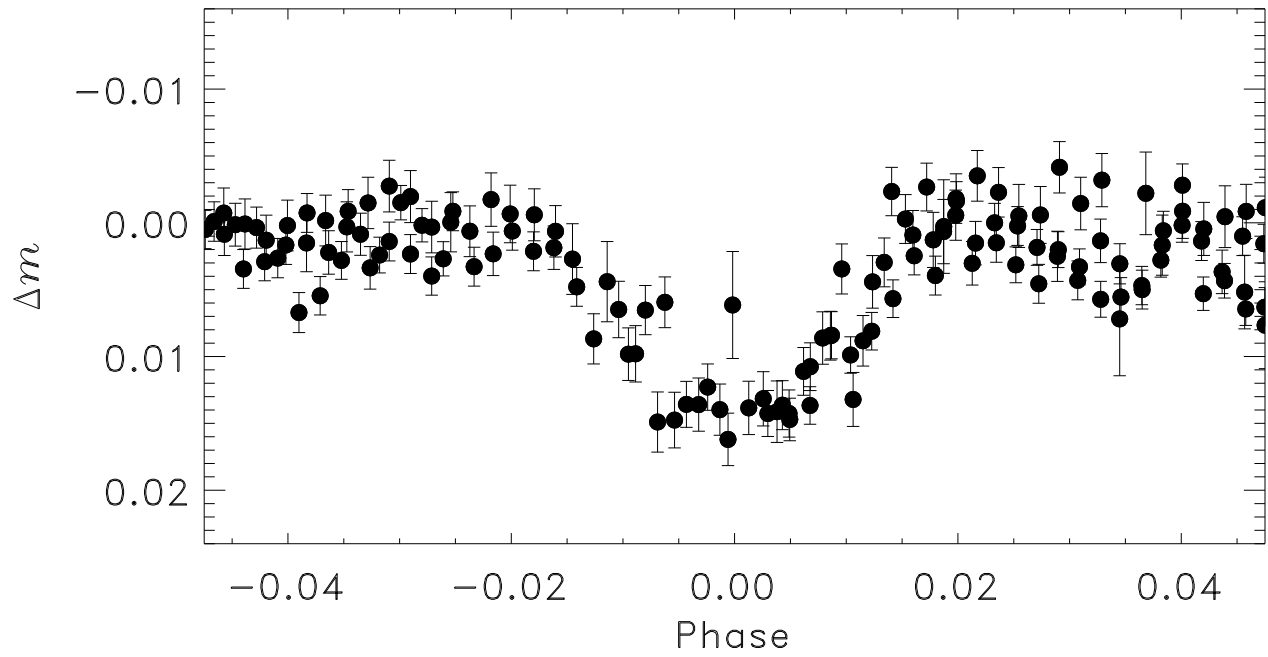


Fig. 2.— Light curves of GSC 01944-02289 obtained from the multicolor photometry of the transits on 2004 March 27 and April 2. The data in consecutive filters are offset by  $-0.05$  for clarity. The typical error of a single point is  $\sim 0.004$  mag.

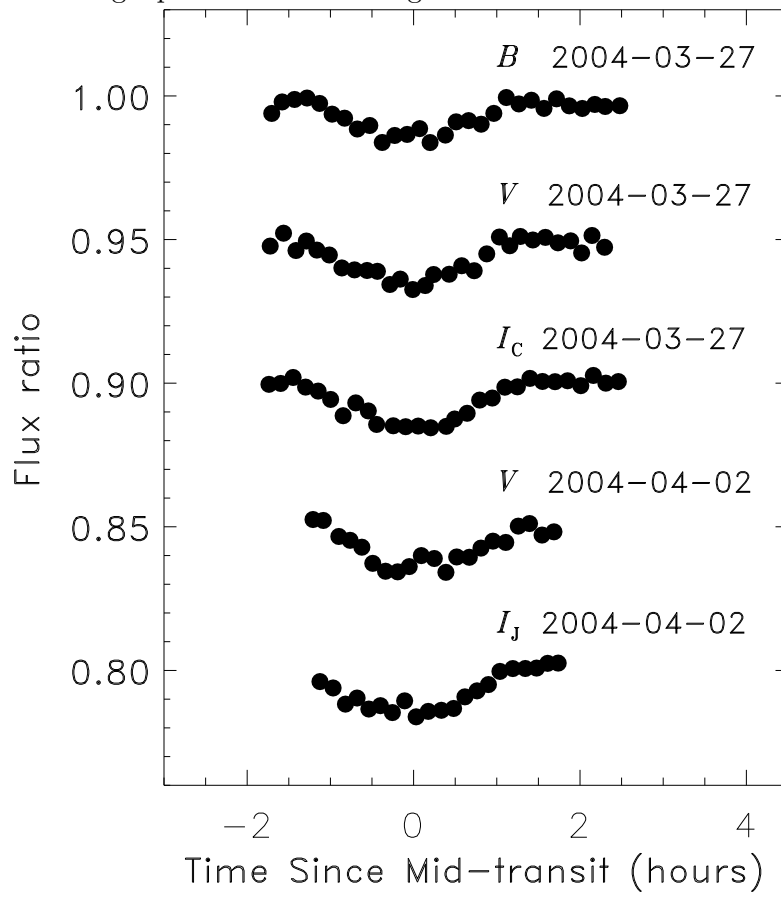


Fig. 3.— Two portions of the observed HIRES spectrum (*diamonds*) of GSC 01944-02289 in the vicinity of the Ca II infrared triplet. The solid line shows the best-fit model spectrum ( $T_{\text{eff}} = 6600$  K,  $\log g = 4.3$ , and  $[M/H] = 0.0$ ). Two additional models are overplotted:  $T_{\text{eff}} = 6000$  K,  $\log g = 4.3$ ,  $[M/H] = 0.0$  (*dotted line*), and  $T_{\text{eff}} = 6600$  K,  $\log g = 3.5$ ,  $[M/H] = 0.0$  (*dashed line*). These fits illustrate the sensitivity of features to  $T_{\text{eff}}$  and  $\log g$ , most noticeably in the wings of the Ca II feature at 866.2 nm.

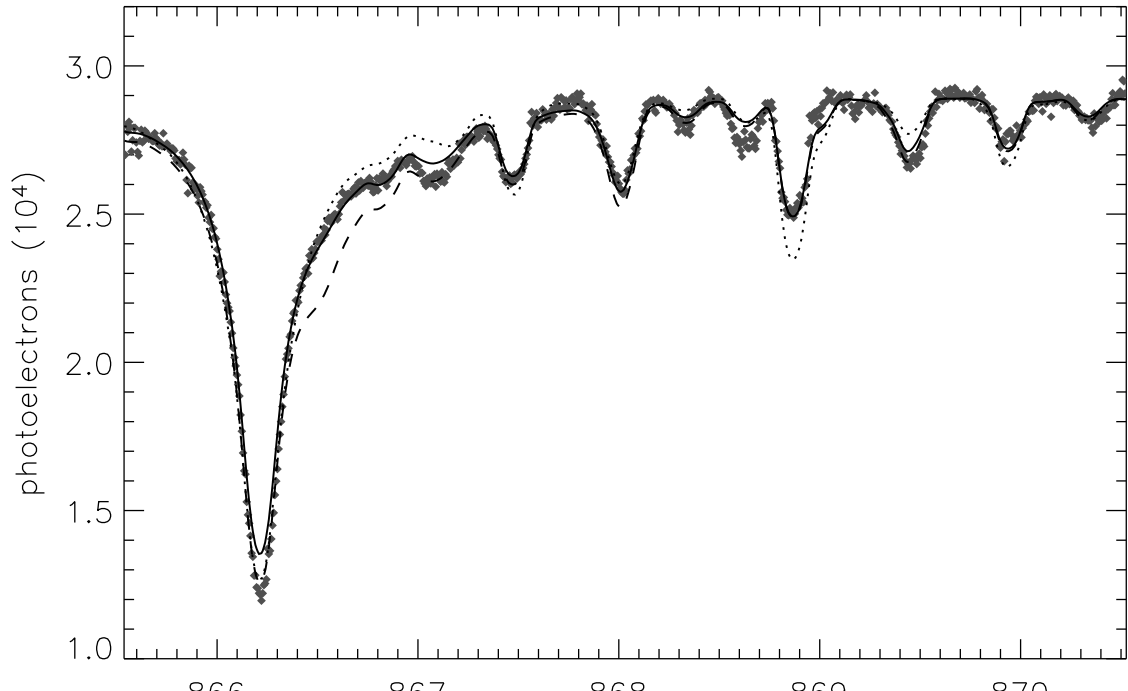
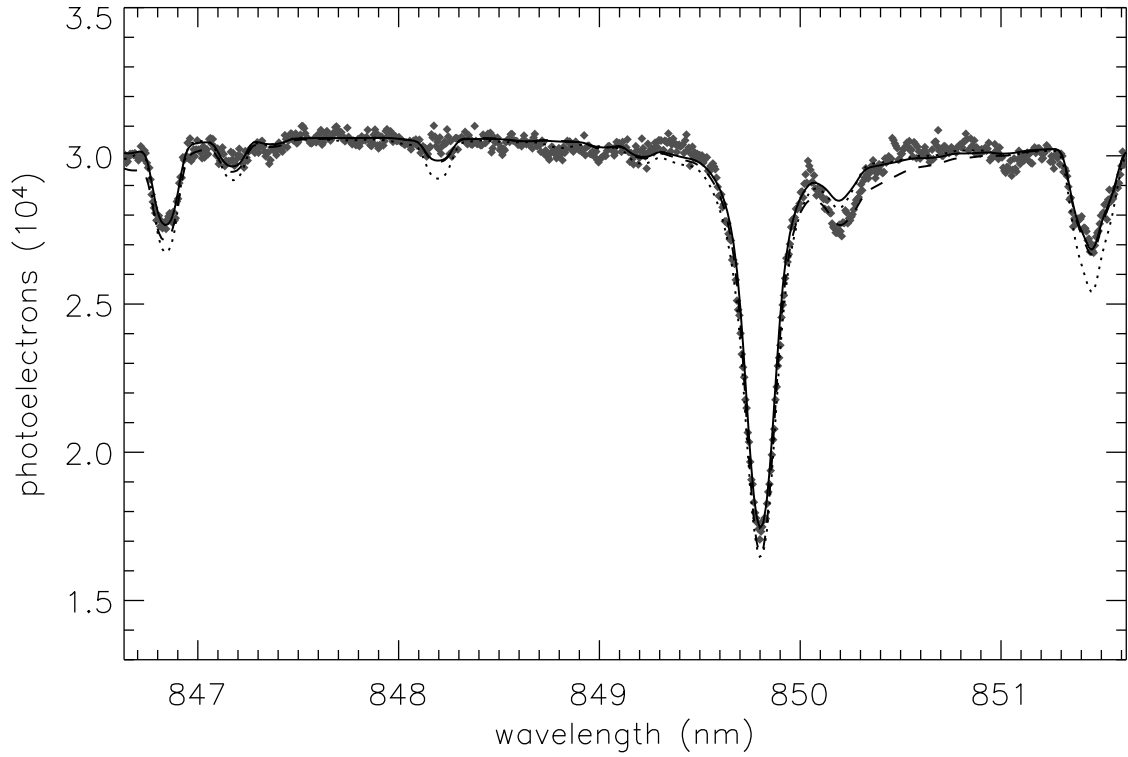


Fig. 4.— Spectroscopic orbit adjusted to the velocities of GSC 01944-02289 using one-dimensional cross-correlations, i.e., under the assumption that the spectrum is single-lined. A circular orbit is assumed, and the ephemeris (period and epoch) are adopted from Eq.[1]. The dotted line represents the center-of-mass velocity. The velocity semi-amplitude of  $3.55 \text{ km s}^{-1}$  implies a brown dwarf companion with a mass of  $32 M_{\text{Jup}}$  (see text), assuming a primary mass of  $1.3 M_{\odot}$ .

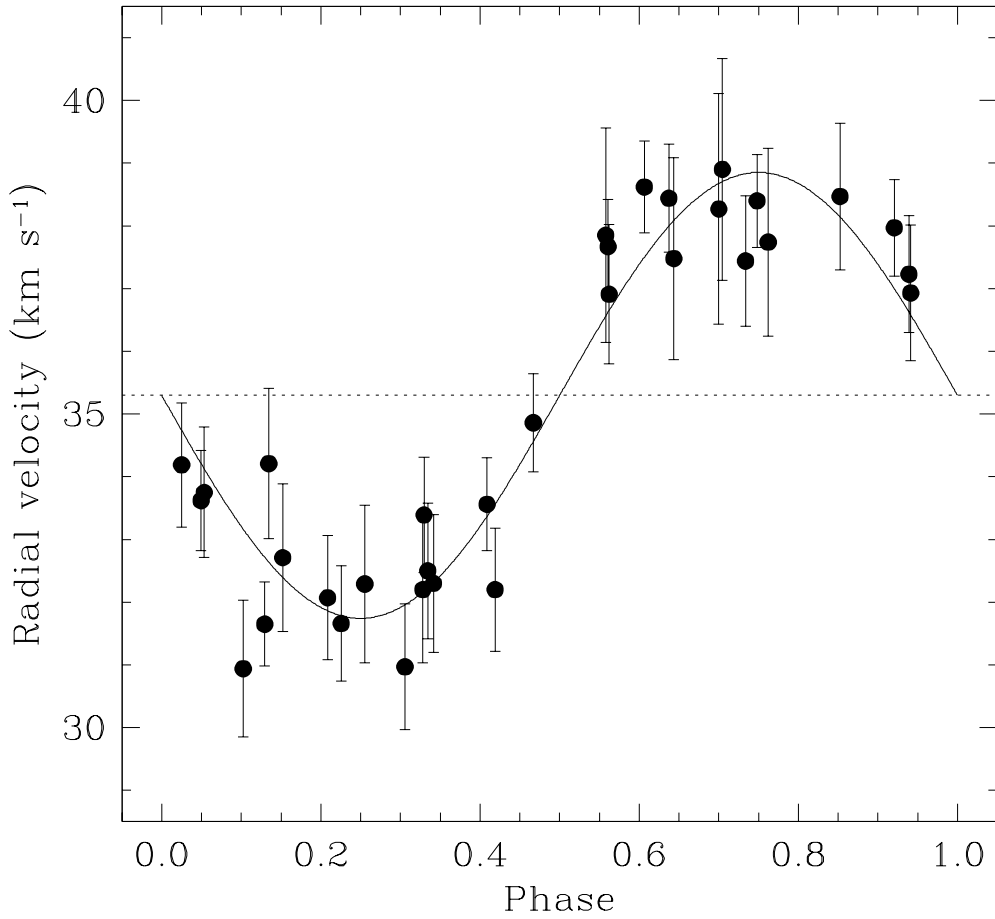


Fig. 5.— (a) Line bisectors for each of our CfA spectra of GSC 01944-02289. The filled circles on each bisector at correlation values of 0.0 and 0.75 indicate the reference levels adopted here for computing the span in velocity. (b) Bisector span used as a proxy for line asymmetry, as a function of orbital phase (see text). One spectrum shows significant contamination by moonlight, and has been omitted. The obvious variations strongly suggest blending with another star.

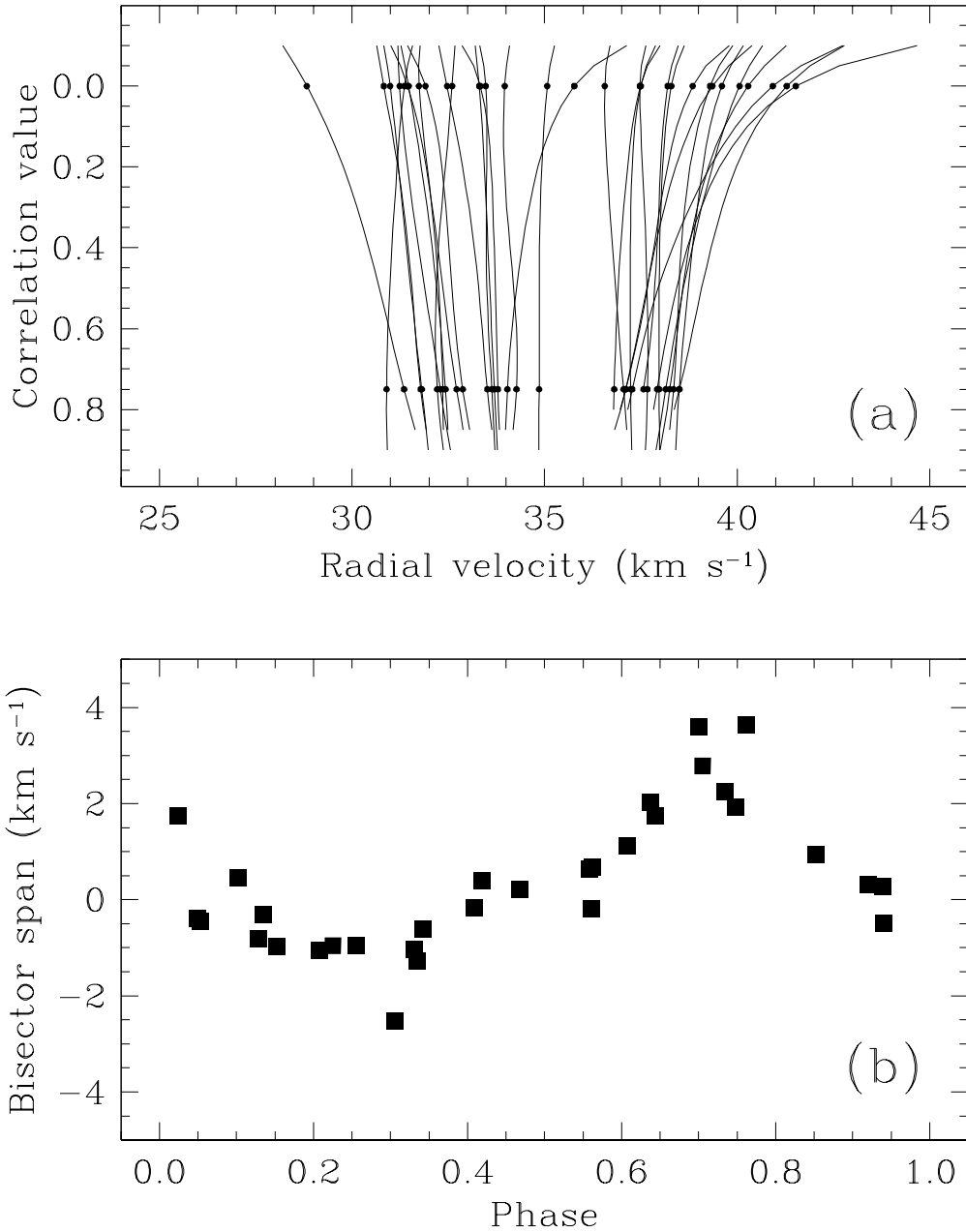


Fig. 6.— Light-curve fit to the wide-field  $R$ -band photometry of GSC 01944-02289, under a blend scenario with an eclipsing binary (G0 star + M3 star) diluted by the light of an F5 star (see text). The bottom panel shows an enlargement in the vicinity of the primary eclipse. A shallow secondary eclipse is predicted (*top panel*) but is undetectable in the present data.

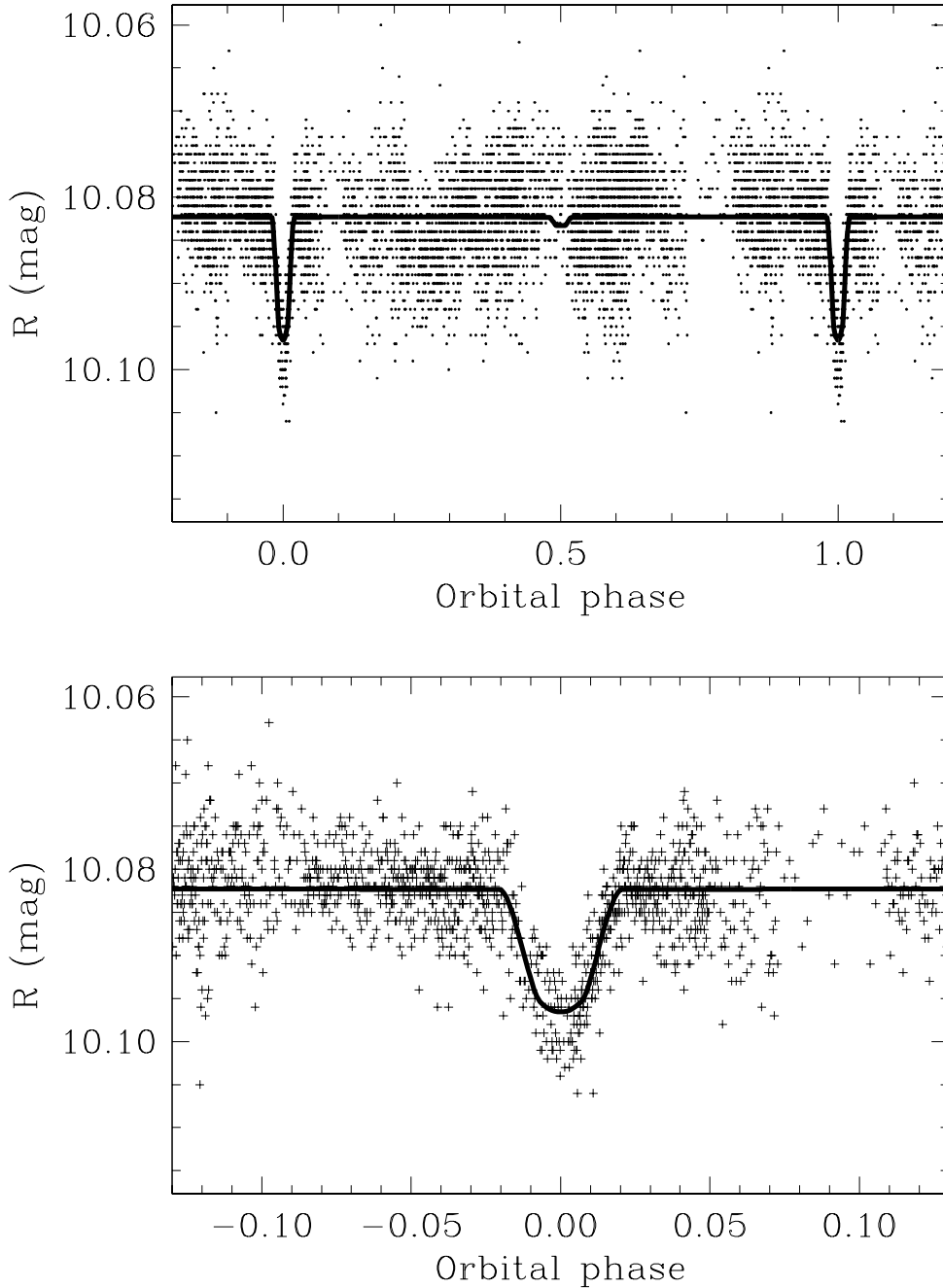


Fig. 7.— Model isochrones from Girardi et al. (2000) for solar metallicity, for ages from 1 to 2.5 Gyr (in logarithmic steps of 0.05 in  $\log t$ , with  $t$  in yr). The isochrone represented by the thick line was found to give the best fit in the blend modeling of GSC 01944-02289 and corresponds to an age of about 1.6 Gyr (see text). The dotted vertical line indicates the spectroscopic constraint on the effective temperature of the brightest star ( $\sim 6500$  K). We represent that star by the large filled circle near the end of the main sequence. The stars composing the eclipsing binary are represented by the two smaller filled circles on the same isochrone.

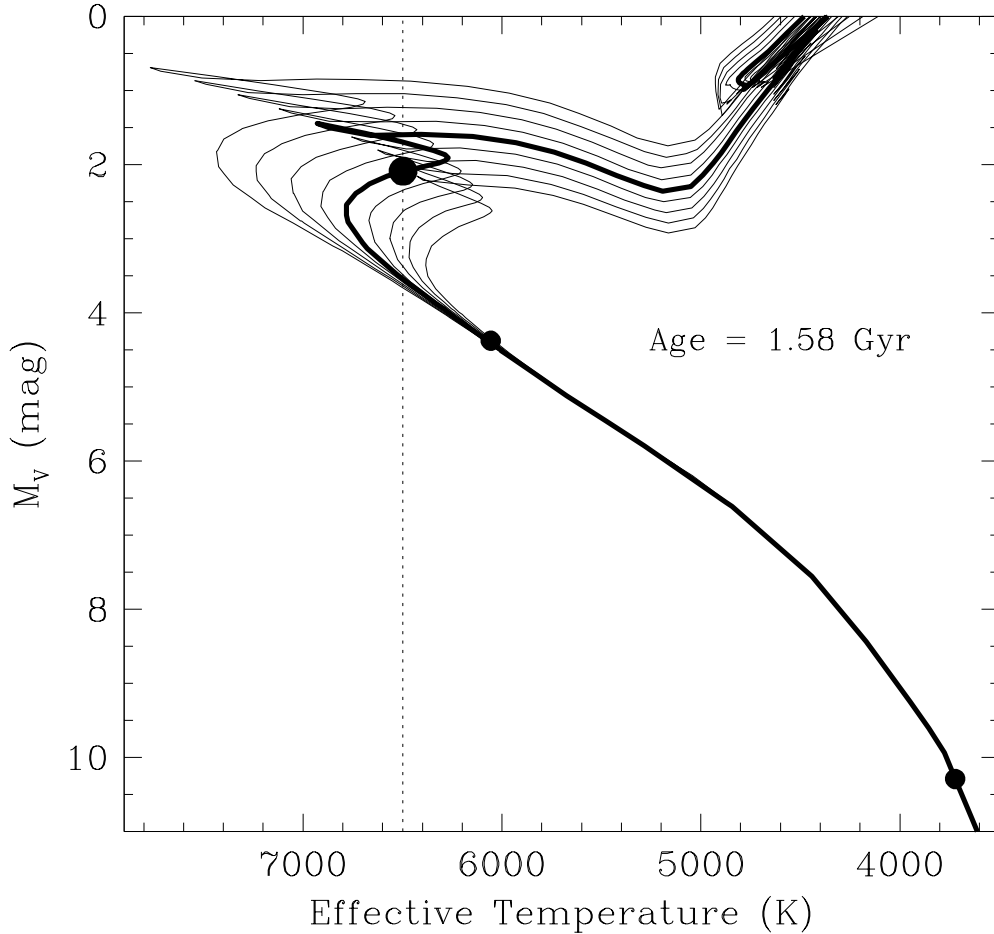


Fig. 8.— Cross-correlation functions from two of our spectra of GSC 01944-02289 obtained near the quadratures. An arrow indicates the expected location of the G star. No obvious sign of that star is seen in the wings of the broadened F star.

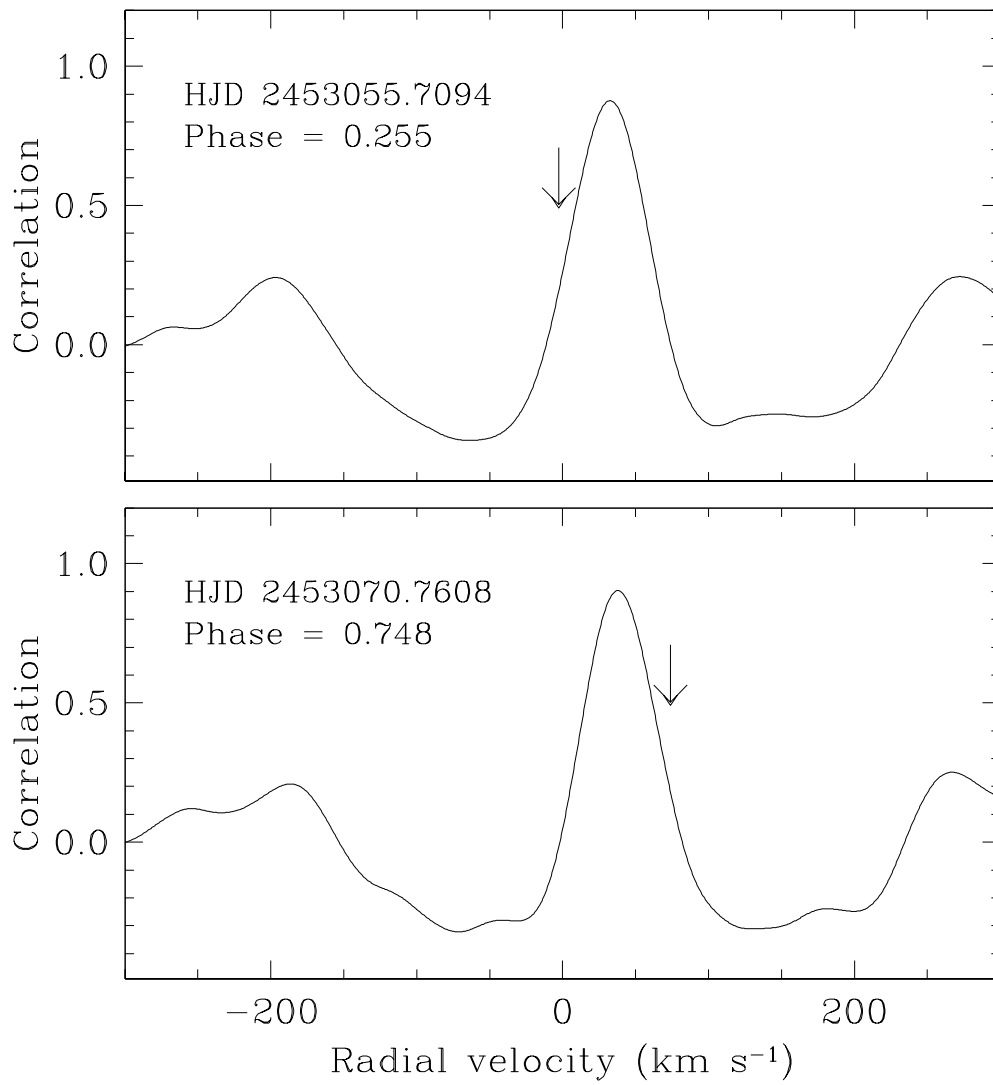


Fig. 9.— (a) Contour diagram of the two-dimensional cross-correlation surface computed with TODCOR as a function of the velocities of the F star and the G star, for one of our spectra of GSC 01944-02289 near phase 0.75 (same spectrum as in the bottom panel of Figure 8). The maximum is indicated by the filled circle, and the dotted lines represent cuts through the surface that are shown in (b) and (c). (b) Cross section of the two-dimensional correlation function at a fixed velocity for the G star, showing a peak corresponding to the F star in GSC 01944-02289. Its measured velocity is represented by the dotted line. (c) Same as (b), but at a fixed velocity for the F star. The peak corresponding to the G star (albeit noisy) is a clear sign of its detection.

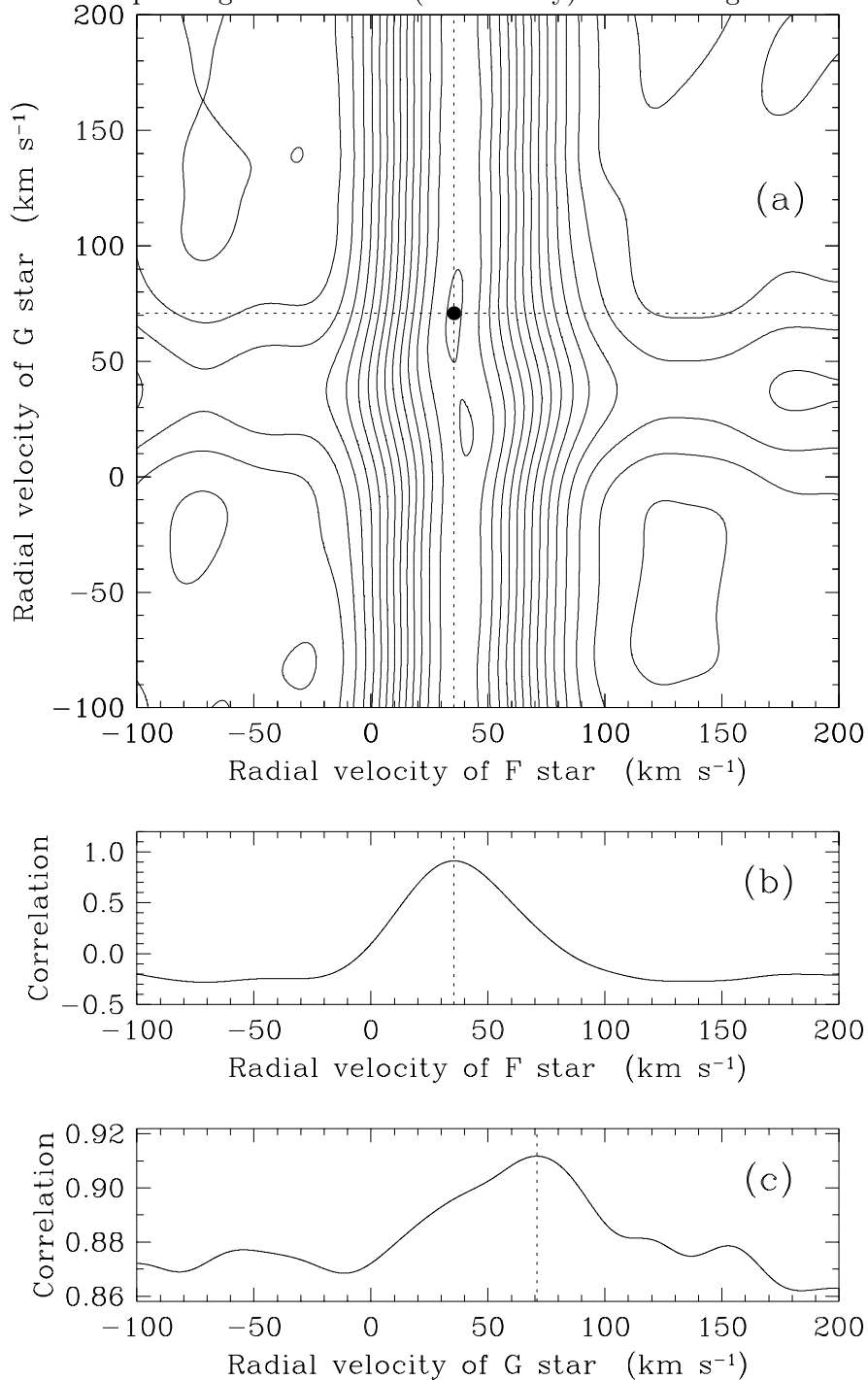


Fig. 10.— Radial velocity measurements from TODCOR for the G star in the eclipsing binary (*open circles*) and the F star (*filled circles*). A spectroscopic orbit has been fitted to the eclipsing binary, assuming zero eccentricity and adopting the ephemeris from Eq.[1]. Shown also for reference is the spurious orbit from Figure 4 for the F star (*dashed line*), which is seen not to fit the new measurements. The center-of-mass velocity of the eclipsing binary is indicated by the dotted line and agrees with the velocities of the F star within the errors (see text).

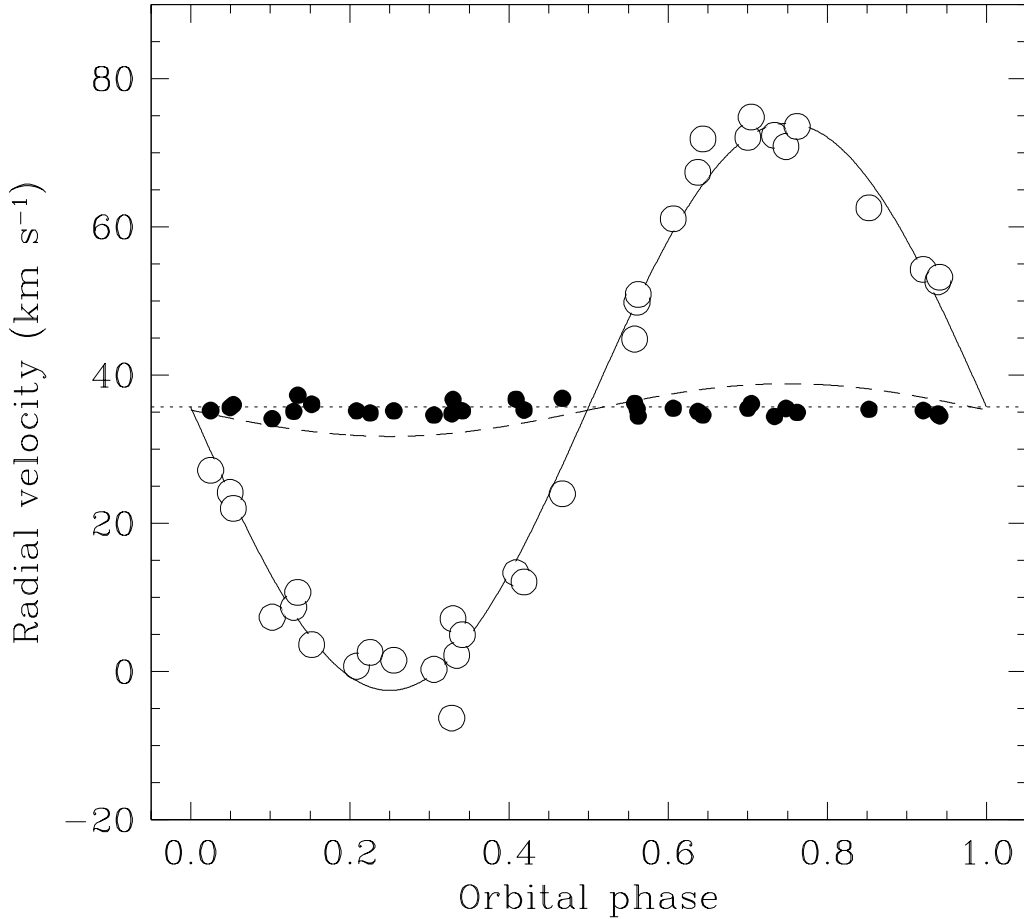


Table 1. Data on GSC 01944-02289

General	Photometry
GSC 01944-02289	$V = 10.357 \pm 0.004$
2MASS 08262257+2659457	$B - V = +0.475 \pm 0.005$
$\alpha = 08^{\text{h}}26^{\text{m}}22^{\text{s}}.6$ (J2000)	$V - R_{\text{C}} = +0.278 \pm 0.008$
$\delta = +26^{\circ}59'46''$ (J2000)	$V - I_{\text{C}} = +0.530 \pm 0.006$
Period = $3^{\text{d}}35002 \pm 0.00002$	$J = 9.478 \pm 0.021$
Depth = $0.014 \pm 0.002$ mag	$H = 9.286 \pm 0.022$
	$K_{\text{s}} = 9.207 \pm 0.021$

Table 2. HIRES spectral standards

Star	Spectral Type	Radial Velocity	Spectral Type/Radial Velocity References
HD 78154A	F6IV	$-2.90 \pm 0.39$	Simbad/de Medeiros & Mayor (1999)
HD 84737	G0.5Va	$+4.90 \pm 0.3$	Keenan & McNeil (1989)/Nidever et al. (2002)
HD 10151	G8V	$-5.65 \pm 0.3$	Keenan & McNeil (1989)/Nidever et al. (2002)

Table 3. Properties of the stars in GSC 01944-02289 composing the blend.

Star	Mass ( $M_{\odot}$ )	$T_{\text{eff}}$ (K)	Radius ( $R_{\odot}$ )	$\log g$ (cgs)	$M_V$ (mag)	$M_{R_{\text{C}}}$ (mag)	$V$ (mag)	$R_{\text{C}}$ (mag)
F star . . . . .	1.68	6497	2.74	3.79	2.09	1.81	10.49	10.21
G star . . . . .	1.12	6055	1.11	4.40	4.38	4.05	12.78	12.45
M star . . . . .	0.36	3721	0.36	4.89	10.29	9.36	18.69	17.76

Table 4. Radial velocity measurements of GSC 01944-02289 (heliocentric frame) measured with TODCOR.

HJD (2,400,000+)	$RV_F$ ( $\text{km s}^{-1}$ )	$RV_{EB}$ ( $\text{km s}^{-1}$ )	$(O-C)_{EB}$ ( $\text{km s}^{-1}$ )	Orbital Phase <sup>a</sup>
53041.7973 . . . .	+34.13	+7.36	-5.41	0.102
53042.8578 . . . .	+35.30	+12.12	-4.95	0.419
53043.8144 . . . .	+36.14	+74.83	+2.42	0.705
53045.8283 . . . .	+34.62	+0.32	+0.53	0.306
53046.6734 . . . .	+36.20	+44.89	-4.44	0.558
53046.6880 . . . .	+34.48	+50.91	+0.61	0.562
53046.8362 . . . .	+35.52	+61.10	+1.66	0.607
53047.6597 . . . .	+35.38	+62.57	-3.75	0.852
53047.8879 . . . .	+35.22	+54.27	+0.23	0.920
53048.6637 . . . .	+36.07	+3.65	-0.84	0.152
53049.7189 . . . .	+36.87	+24.00	-3.85	0.467
53050.4997 . . . .	+35.53	+72.08	-0.01	0.700
53052.6484 . . . .	+35.18	+4.98	+1.36	0.342
53054.6574 . . . .	+34.50	+53.23	+3.71	0.941
53055.7094 . . . .	+35.18	+1.54	+4.05	0.255
53058.6548 . . . .	+37.28	+10.72	+3.61	0.134
53059.5737 . . . .	+36.76	+13.34	-1.63	0.409
53060.7572 . . . .	+34.96	+73.56	-0.29	0.762
53061.6383 . . . .	+35.22	+27.17	-2.55	0.025
53062.6745 . . . .	+35.45	+2.23	-0.49	0.334
53070.7608 . . . .	+35.51	+70.86	-3.10	0.748
53071.7702 . . . .	+35.62	+24.18	+0.16	0.049
53072.7035 <sup>b</sup> . . .	+34.79	-6.24	-8.22	0.328
53073.7394 . . . .	+35.10	+67.39	+2.63	0.637
53074.7501 . . . .	+34.73	+52.63	+2.61	0.939
53075.6526 . . . .	+35.19	+0.74	+1.97	0.208
53076.8331 . . . .	+35.46	+49.83	-0.14	0.561
53127.6627 . . . .	+34.44	+72.37	-1.39	0.734
53128.7340 . . . .	+36.01	+22.02	-1.08	0.053
53129.6589 . . . .	+36.73	+7.14	+4.99	0.330
53130.7108 . . . .	+34.61	+71.89	+6.17	0.644
53132.6602 . . . .	+34.89	+2.60	+4.68	0.225
53135.6883 . . . .	+35.11	+8.70	+0.76	0.129

<sup>a</sup>Referred to the ephemeris of Eq.[1].

<sup>b</sup>The observation taken on this date shows the largest velocity residual, and happens to be contaminated by moonlight. It is the same observation omitted from Figure 5.

Table 5. Predicted total apparent magnitudes from our blend model for GSC 01944-02289, compared with the measured brightness in the optical and near infrared.

Passband	Predicted brightness <sup>a</sup> (mag)	Observed brightness (mag)	O–C difference (mag)
<i>B</i> . . . . .	10.844	10.832	–0.012
<i>V</i> . . . . .	10.364	10.357	–0.007
<i>R<sub>C</sub></i> . . . . .	10.079	10.079	0.000
<i>I<sub>C</sub></i> . . . . .	9.807	9.827	+0.020
<i>J</i> . . . . .	9.462	9.478	+0.016
<i>H</i> . . . . .	9.285	9.286	+0.001
<i>K<sub>s</sub></i> . . . . .	9.217	9.207	–0.010

<sup>a</sup>The *JHK* magnitudes from the Girardi et al. (2000) models have been converted to the 2MASS system for comparison with the observed quantities, following Carpenter (2001).